



Oscar, L., Nzau, M. J., Ellen, D., Franklin, O., Rachel, J., Richard, W., & Tom, W. (2022). Characteristics of the Turkana low-level jet stream and the associated rainfall in CMIP6 models. *Climate Dynamics*.  
<https://doi.org/10.1007/s00382-022-06499-4>

Publisher's PDF, also known as Version of record

License (if available):  
CC BY

Link to published version (if available):  
[10.1007/s00382-022-06499-4](https://doi.org/10.1007/s00382-022-06499-4)

[Link to publication record in Explore Bristol Research](#)  
PDF-document

This is the final published version of the article (version of record). It first appeared online via Springer at <https://doi.org/10.1007/s00382-022-06499-4> .Please refer to any applicable terms of use of the publisher.

## University of Bristol - Explore Bristol Research

### General rights

This document is made available in accordance with publisher policies. Please cite only the published version using the reference above. Full terms of use are available:  
<http://www.bristol.ac.uk/red/research-policy/pure/user-guides/ebr-terms/>



# Characteristics of the Turkana low-level jet stream and the associated rainfall in CMIP6 models

Lino Oscar<sup>1,3</sup> · Mutemi J. Nzau<sup>1</sup> · Dyer Ellen<sup>2</sup>  · Opijah Franklin<sup>1</sup> · James Rachel<sup>2,4</sup> · Washington Richard<sup>2</sup> · Webb Tom<sup>5</sup>

Received: 11 January 2022 / Accepted: 2 September 2022  
© The Author(s) 2022

## Abstract

The Turkana low-level jet stream (TJ) is important to climatic conditions over northern Kenya and East Africa. The representation of the TJ in climate models varies due to the TJ interaction with Turkana channel that is influenced by model resolution and influences the model representation of the regional climate. This study compares features of the TJ in CMIP6 AMIP model simulations with ERA5. Models reveal climatological wind speeds that match those of the reanalysis from the ERA5 at the jet entrance (13 m/s) but lower magnitudes of wind speed and vertical shears compared to ERA5 within the Turkana channel. The models with slowest wind speeds, have a flattened Turkana channel and fail to exhibit the terrain constriction at 37° E which otherwise aids in accelerating winds to form a jet core. Furthermore, they fail to represent the narrowing of the channel as in ERA5, thereby forming blocking walls in the channel, forcing vertical ascent and mixing, and weakening shear. This boosting of ascent motion promotes rainfall formation and enhances wet anomalies at the exit of the TJ when the jet stream is weaker. By applying a new narrowing index, we demonstrate the need to improve topography details in the CMIP6 models, particularly those with resolution coarser than 1.5°, in order to properly simulate the TJ and the observed rainfall over the northwestern areas of eastern Africa.

**Keywords** Turkana low-level Jet stream · ERA5 · CMIP6 · Atmospheric models · East Africa rainfall

## 1 Introduction

Over northern Kenya, there exists a low-level jet stream which has great socio-economic potential for the region, as well as being an important mechanism for moisture transport from the western Indian Ocean to some interior parts of northwestern East Africa (Vizy and Cook 2019; Nicholson 2014). This fast-flowing current of air, referred to as the Turkana low-level Jet stream (TJ), gained recognition among aviators who frequently experienced turbulence

when landing and taking off from the region (Indeje et al. 2001). The understanding of the TJ benefited from short field campaigns by Kinuthia and Asnani (1982) and Kinuthia (1992). Occasional ascents of pilot balloons during field campaigns in Kinuthia (1992) indicated the TJ is strongest during late night and early morning, with associated wind speeds in the range of 30–50 m/s. The TJ is fragmented into two branches in the channel which merge at the mid-portion of the channel to form a jet core (Kinuthia and Asnani 1982; Indeje et al. 2001). The mean monthly wind speeds in range 10–13 m/s culminate at 850 mb (Nicholson 2016) from January to December. Previous studies have related the TJ with the observed aridity over parts of Eastern Africa due to the stable atmospheric conditions associated with large scale dynamics of the low-level jet stream (e.g., Trewartha 1981; Nicholson 1996, 2016; Ba and Nicholson 1998; Sun et al. 1999; Indeje et al. 2001). It is for this reason that the inclusion of the TJ in dynamical models is important to the representation of rainfall over the northern Kenya region (Sun et al. 1999; Indeje et al. 2001; King et al. 2021).

---

✉ Dyer Ellen  
ellen.dyer@ouce.ox.ac.uk

<sup>1</sup> University of Nairobi, Nairobi, Kenya

<sup>2</sup> School of Geography and the Environment, University of Oxford, Oxford, UK

<sup>3</sup> Kenya Red Cross, Nairobi, Kenya

<sup>4</sup> School of Geographical Sciences, University of Bristol, Bristol, UK

<sup>5</sup> Shell, London, England, UK

Eastern Africa (EA) is a generally dry region, found in an otherwise wet equatorial belt (Camberlin 2018). The region is hyper-arid at the tip of the Horn and near the Egyptian border with annual rainfall below 150 mm (Njenga et al. 2014), an apparent extension of desert conditions from the bordering middle-East and Sahara respectively. An extensive area featuring less than 400 mm annual rainfall stretches from eastern Ethiopia through northwestern Kenya, to Lake Turkana (Nicholson 2016; Camberlin 2018). Extreme drought events have been common, exacerbated by modes of variability that perturb rainfall received, whose manifestations have increased notably since 2005. Between 1975 and 2018 alone, five drought events occurred in the latter seven years (2005/2006, 2008/2009, 2010/2011, 2015/2016, 2016/2017) compared to only seven events in former 30 years (1975 and 2004). The 2015 and 2016 drought over most parts of Ethiopia related to El Nino conditions (Philip et al. 2018), while 2016 and 2017 drought over the Greater Horn related to La Nina (Uhe et al. 2018). Further work by Preethi et al. (2015) indicates that the canonical El Nino and the El Nino Modoki are associated with depressed rainfall southern hemispheric regions and enhances the rainfall in northern areas of East Africa during March to May (MAM) season. However, during the October to December (OND) season, it is the canonical El Nino and positive Indian Ocean Dipole that are associated with the enhancement of rainfall over Eastern Africa. Trend analysis suggests that these perturbations are becoming frequent as the large-scale Walker circulation is intensifying (McGregor et al. 2014), although different models exhibit biases in the Walker Circulation (King et al. 2020). The increased manifestation of drought impacts has heightened interests in climate information from models to inform disaster risk management and increase people's adaptive capacity to climate extremes (Nicholson 2014; Kilavi et al. 2018).

Increased studies on the TJ using the current generation of climate models and improved datasets can lead to better understanding of the TJ as well as its impacts. The aridity is linked to regional topography and wind flow. Due to the north–south orientation of the east African highlands, advection of moist air from Congo-basin into the arid area is blocked (Slingo et al. 2005). Lower-tropospheric (at 850 mb level) divergence matched by subsidence at mid troposphere characterizes the arid sub-regions (Yang et al. 2015). The large-scale divergence is linked with the TJ as fast-moving winds cause a drop in pressure due to Bernoulli effect (Indeje et al. 2001) and interact with terrain within the channel, inducing frictional divergence. The divergence in the lower atmosphere leads to formation of stable atmospheric conditions, resulting into a shallow moist layer and a dry climate over the Turkana channel and its flanks including Kenya and Somali border, the Nile plains of Sudan and South Sudan (Trewartha 1981; Ba and Nicholson 1998; Nicholson 2016).

The TJ also transports moisture that promote rainfall formation at the jet exit in western South Sudan and Ethiopia and shifts rainfall regime from eastern South Sudan during the northern summer (Vizy and Cook 2019). The strength of the TJ covaries with the ENSO system that drives rainfall over East Africa during October to December (Nicholson 1996; Sun et al. 1999; King et al. 2021).

Acosta and Huber (2017) examine the ability of the Community Atmosphere Model to correctly simulate low-level jets over the Indo-Gangetic Plain, and found the model had a good representation, which they attribute to proper representation of model physics schemes that explicitly resolve the Indo-Asian monsoon. Investigating the National Center for Atmospheric Research (NCAR) model at a grid resolution of 0.5°, Indeje et al. (2001) reported a fairly good representation of the features in the TJ compared with the observations in Kinuthia (1992). A comparison of how several climate models simulate the TJ has been made, indicating that the models follow similar seasonal pattern as the ERA5 and MERRA2 reanalysis with more comparable values from January to May than in the remaining months of the year in CMIP5 (King et al. 2021). While in the seasonal cycle the TJ is strong during the two major rainfall seasons in East Africa (MAM and OND), its strong anomalies are accompanied by dry conditions in its area of influence. Munday et al. (2021) suggests that the CMIP5 models with horizontal resolution of more than 60 km do not replicate the associated dry anomalies as finer grid lengths are required to accurately simulate the TJ and its interaction with East African climate. However, reasons for why the models represent the TJ the way they do, including the influence of the TJ on the airflow over the region, and how this affects the weather over the region in models, is not well understood. Furthermore, there have been no previous studies of the simulation of the TJ in the newest generation of global models.

This work focuses on characteristics of the TJ in CMIP6 models. Specifically, it discusses model representation of the strength, structure and position of TJ along the Turkana channel which may affect the simulated rainfall. We recognize that model simulation of these features introduces a measure of uncertainty because of the lack of observational datasets. But since it is understood that some low-resolution models ignore low-level jet streams (Acosta and Huber 2017), there is the opportunity to refine our understanding of the jet stream characteristics and influence on rainfall by using the recently available CMIP6 and ERA5 with high spatial resolution. While development in modeling is a continuous process and better products are getting available, there is the need to understand model uncertainties and build confidence in them. Through evaluating the model representation of a key feature to rainfall in the region, this study informs both model development process and model use (James et al. 2017). The current work will investigate the

following (a) What are the climatic characteristics of the TJ in different climate models? (b) How might resolution and the representation of topography in the models be related to these differences? (c) Is the simulated rainfall related to these differences?

Atmospheric models and reanalysis datasets used, as well as methods for locating and quantifying key features of the jet stream are described in Sect. 2. Results from analysis that characterize the TJ in CMIP6 models, associate the simulated TJ to topography and relate rainfall in CMIP6 to the TJ are shown in Sect. 3. A summary is provided in Sect. 4 and conclusions drawn in Sect. 5.

## 2 Data and methods

### 2.1 Datasets

This study makes use of the data from the sixth iteration of the Coupled Model Intercomparison Project (CMIP6; Eyring et al. 2016) under the World Climate Research Programme (Taylor et al. 2012). The historical Atmospheric Model Intercomparison Project (AMIP), which is one of the

four baseline experiments from CMIP6, were considered for a period between 1980 and 2014. Twenty-six atmospheric models (Table 1) were analyzed, which were the models with all variables needed for this analysis. The historical AMIP runs were chosen for this analysis as they assume the historical sea surface temperature (SST) input into the experiments. Consequently, they may reduce uncertainties related with SST feedback (Eyring et al. 2016) and allow for oscillations in the output data to be matched with the atmospheric reanalysis for a period 1981 to 2014. The resolution of the models differs but the analysis was performed on the models' native grid to preserve the original information. Among the models used, 4 were drawn from the High-Resolution Model Intercomparison Project (HighResMIP) and 22 were regular experiment models. HighResMIP models are designed to represent climate processes with global model resolutions (~ 25 km). HighResMIP models used in this study included HadGEM3-GC31-MM, MPI-ESM1-2-HR, IPSL-CM6A-LR and CNRM-CM6-1.

To benchmark the findings by the models, this study takes advantage of the latest reanalysis dataset from the fifth version of European Centre for Medium-Range Weather Forecasts reanalysis—ERA5 (Hersbach et al. 2020). In ERA5,

**Table 1** Name and description of CMIP6 models used in this study, including resolutions for the model runs

Modeling center	Model	Atmospheric horizontal resolution (lat × lon °)
AS-RCEC	TaiESM1	0.94 × 1.25
BCC	BCC-ESM1	1 × 1.25
	BCC-CSM2-MR	0.94 × 1.25
CAMS	CAMS-CSM1-0	0.94 × 1.25
CAS	FGOALS-g3	1.39 × 1.41
	FGOALS-f3-L	1.39 × 1.41
CCCma	CanESM5 <sup>2</sup>	1.39 × 1.41
CNRM-CERFACS	CNRM-CM6-1	0.56 × 0.83
	CNRM-ESM2-1	1.25 × 1.88
CSIRO	ACCESS-CM2	1.25 × 1.88
	ACCESS-ESM1-5	1.25 × 1.88
INM	INM-CM5-0	5.18 × 2
	INM-CM4-8	1.85 × 1.88
IPSL	IPSL-CM6A-LR	1.11 × 1.13
MPI-M	MPI-ESM1-2-HR	1.11 × 1.13
MIROC	MIROC6	1.5 × 2
MOHC	HadGEM3-GC31-LL	1 × 1.25
	HadGEM3-GC31-MM	0.93 × 0.94
MRI	MRI-ESM2-0	1.11 × 1.13
NCAR	CESM2	1.89 × 2.5
NCC	NorESM2-LM	1.27 × 2.5
	NorCPM1	1.89 × 2.5
NOAA/GFDL	GFDL-CM4	0.94 × 1.25
NUIST	NESM3	2.77 × 2.81
SNU	SAM0-UNICON	2.77 × 2.81

the 2000–2017 climatological wind speeds associated with the TJ matches well with structures found using NCEP CFSR reanalysis dataset (Hartman 2018), and MERRA2 dataset although the TJ is stronger in MERRA2 during early months of the year (Vizy and Cook 2019). However, the climatological wind speeds in the ERA5 are comparable, albeit slower than 31 m/s that was occasionally recorded in the July 1979 to June 1980 single year of field observations in Kinuthia (1992). This disparity is hypothesized to be as result of terrain features of smaller scale that are not resolved in the reanalysis at the horizontal resolution of  $0.25^\circ$ .

## 2.2 Methods

We discuss the methodology used to quantify the seasonal cycle of the TJ, its spatial structure, the detection threshold of the TJ, the narrowing index (representing shape of the Turkana channel), and the precipitation index. The seasonal cycle represents physical characteristics of the TJ which presented as the range of wind speed values in climatology at TJ core. The spatial structure of the TJ is determined in wind profiles for the cross section through the Turkana channel, which is at the point  $2^\circ$  S,  $43^\circ$  E to the point  $8^\circ$  N,  $32^\circ$  E. Those points were used by Nicholson (2016) to mark the cross-sections. In this work, the TJ exit coincided with a point beyond which the wind was slower than 5 m/s. The winds were found to accelerate in the mid-portion of the Turkana channel particularly in October to May season depicting a jet core. Finally, the jet entrance marked the point of entry of winds into the Turkana channel.

Another aspect of the seasonal cycle was studied in the shift in direction of the TJ. This was determined by assessing the prevailing wind vectors over East Africa, which shift direction from southerly to northerly, following the apparent movement of the overhead sun in a year. The horizontal extent of the TJ was identified in both the reanalysis and models by masking the mean wind for speed of magnitudes less than 5 m/s, a value marking minimum value for range of the ensemble range. The ensemble range was computed as  $\pm$  one standard deviation of the 26 models in each month around the ensemble mean. The resultant wind vectors at the 850 mb level provided a key map showing the relatively high-speed winds with an axis confined within the Turkana channel in reanalysis and most of CMIP6 models. This matched the observational work of Kinuthia and Asnani (1992) who reported that the TJ culminates in the layers 925 and 700 mb with wind speeds of about 13 m/s within the Turkana channel.

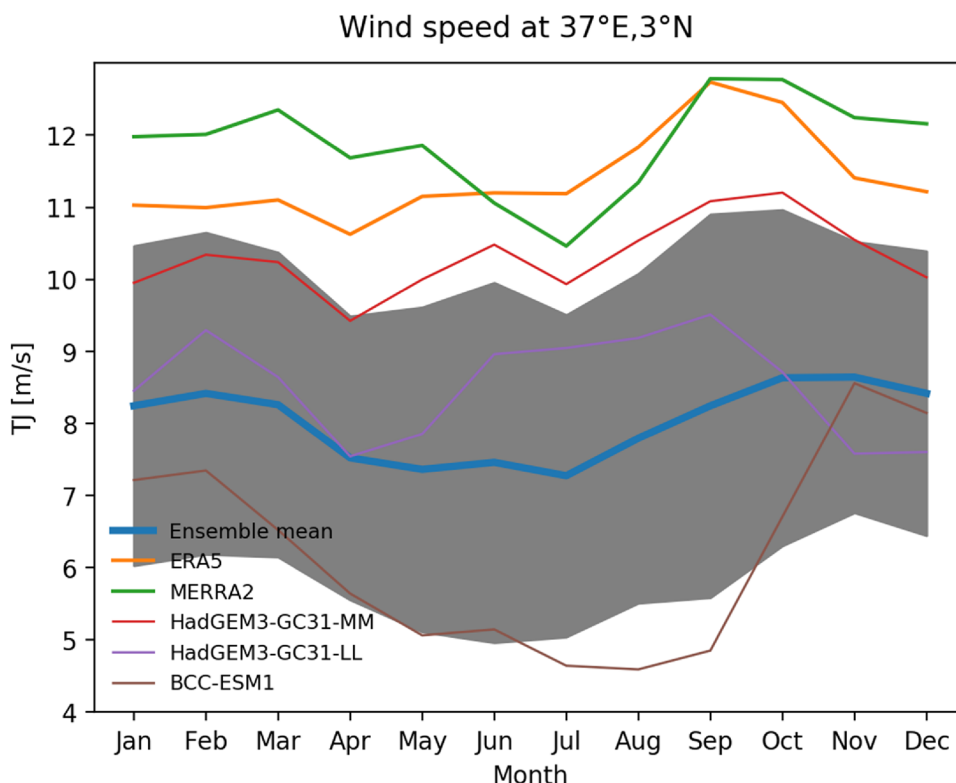
The threshold for occurrence of the TJ was identified when the structures of the cores of the TJ in the model matched those in the ERA5 datasets. A search criterion was applied to the wind speed at  $37^\circ$  E,  $3^\circ$  N for mean JJAS seasons over the period of 35 years to identify optimal

thresholds for a strong and well-formed TJ. Thresholds for maximum winds at 850 mb level were searched in range 6 m/s and 12 m/s, along with thresholds for wind shears in range 2 m/s and 6 m/s. Shear was taken as the difference between maximum wind speed (at 850 mb) and minimum wind speed found at any level above the 850 mb, searching before 500 mb level is reached. The Optimum thresholds of maximum wind speed and shear for the TJ during JJAS in the models is that which the majority of the models, especially those of higher resolution with a well-formed Turkana channel (described by index of narrowing) that maintains it. The thresholds applied in studying the TJ were less stringent than those applied on ERA-Interim dataset (maximum wind speed 10 m/s, matched with decreasing wind speeds aloft in 2–4 m/s in Nicholson 2016) and those postulated by Oliveira et al. (2018), which were found too stringent to capture a TJ in the models.

Maintenance of the TJ is attributed to confinement of winds along the Turkana channel (Kinuthia 1992; Indeje et al. 2001; Nicholson 2016; Vizy and Cook 2019). Its intensification in CMIP6 models is linked with the topography through the narrowing index. This is estimated as the mean change in the cross-sectional area of the channel. The cross-sectional area was obtained by estimating the area under a curve between constant height at 850 mb and the surface along a longitude. The cross-sectional area was calculated along each longitude for the longitudes  $33^\circ$  E (marking the exit of the jet stream) to  $42^\circ$  E (marking the entrance of the jet stream), and bounded by the latitudes  $2^\circ$  S and  $9^\circ$  N. The narrowing index summarizes the consistency in narrowing towards the constriction at the mid-portion of the Turkana channel, and indicates the relative ease of air mass to flow through the channel without being blocked and being accelerated to form an intense TJ core in accordance with Bernoulli's principle (Indeje et al. 2001).

The influence of the jet in CMIP6 is linked to East African climate through the precipitation index. Precipitation index is computed for climatological precipitation associated with the TJ in CMIP6 models. The index is obtained as composite means for TJ occurrences, and no-TJ occurrences for rainfall at each grid box. These TJ events were isolated from the 35 years of analysis by identifying when the core wind speeds in the TJ reached the detection threshold of the TJ during JJAS season. This season matches when moisture is high at the TJ exit region as it is the main rainfall season over the north-western parts of East Africa (Camberlin 2018).

**Fig. 1** The 1980–2014 mean wind speeds in reanalysis datasets (ERA5 and MERRA2), three CMIP6 models (HadGEM3-GC3-MM, HadGEM3-GC3-LL and BCC-ESM1) and the 26 CMIP6 model (shown in Table 1) ensemble at the 850 mb level in each month of the year for the grid closest to 37° E, 3° N (green dot shown in Fig. 2). Gray shaded region denotes the range of values for climatology in CMIP6 models (computed as  $\pm$  one standard deviation of the 26 models in each month around the ensemble mean)



### 3 Results

#### 3.1 Seasonal cycle of the TJ in CMIP6 model climatology

The mean wind speeds for 1980–2014 are shown for a point at mid Turkana channel (Fig. 1). In ERA5 and MERRA2, they remain relatively high throughout the year with mean values ranging between 10 and 13 m/s. The MERRA2 emphasizes on existence of a peak in March and higher one in September, which is also exhibited in ERA5, matched by a low in July. In different reanalysis (MERRA2, ERA5, and JRA-55) datasets, the TJ has similar peak and low seasons although with a bias from each other (Vizy and Cook 2019; King et al. 2021). While TJ strength is similar in September, it is stronger in MERRA2 during March, and weakest between April and October in JRA-55, among the three datasets (King et al. 2021).

The HadGEM-GC31 models similarly have about a 2 m/s range between maximum to minimum values as depicted in ERA5 and MERRA2, albeit the peak and low magnitude of the models is lower. Most variation between the different CMIP6 models is exhibited between May and October. In this period also, the spread of individual model values about the ensemble is minimal, indicating that most of the models agree. Despite this agreement, they exhibit

relatively lower values compared with reanalysis data. During the same months, the BCC-ESM1 model exhibited categorically low mean wind speeds, ranging between 5 and 9 m/s with particularly low values from April to September. While it has been suggested that model resolution can determine the TJ representation (Indeje et al. 2001), this result shows that with similar resolution as HadGEM-GC31-LL, the TJ in BCC-ESM1 (see Table 1) is weaker with different seasonal cycles. This work explores what might be the drivers for these differences.

The TJ characteristics are further explored, in the four datasets in a year by masking wind vectors for winds speeds below 5 m/s at 850 mb level. The pressure level is chosen since the wind here flows above the terrain and therefore, it is the lowest level of the TJ which is free from obstruction by the terrain barrier. Figure 2 shows the mean wind vectors in reanalysis (ERA5 and MERRA2) and wind from 2 CMIP6 models chosen. High wind speeds of at least 5 m/s in both reanalysis and the HadGEM-GC31 are constrained within the Turkana channel throughout the year. The BCC-ESM1 model has the winds spread out over Kenya.

In the year, the background flow shifts from southerly during May to September, to northerly during October to April while the winds within Turkana channel remains southeasterly, showing directional consistency. The southerly flow during May to September splits over northern Kenya, into two streams: south-easterly flow (the TJ), and

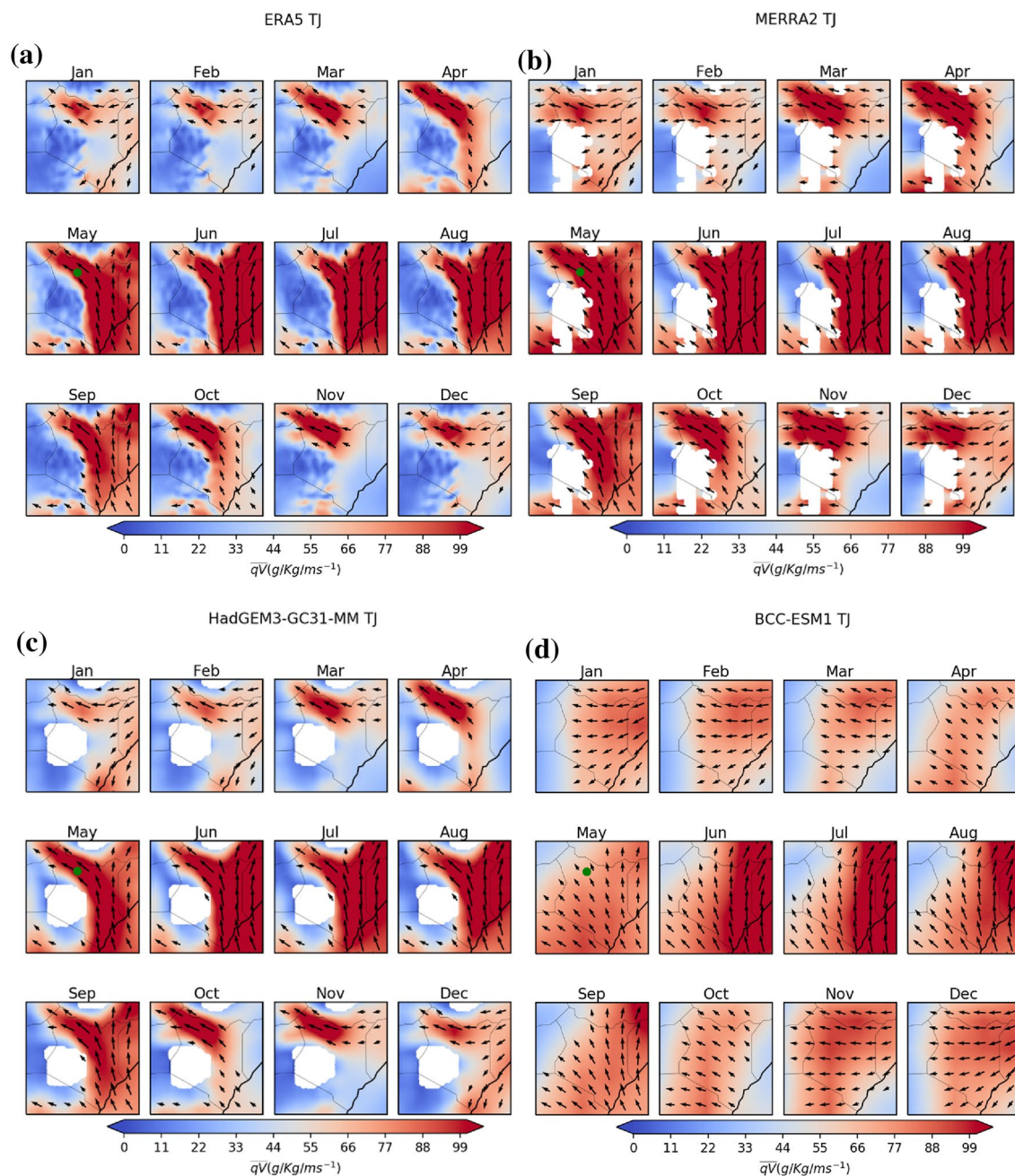


**Fig. 2** The 1980–2014 climatological moisture flux at 850 millibars ( $\text{g/Kg/m/s}$ ), overlaid with mean wind vector at 850 millibars ( $\text{m/s}$ ) for ERA5, MERRA2 and two CMIP6 models (HadGEM3-GC3-MM

and BCC-ESM1). Wind vectors indicate winds of at least 5  $\text{m/s}$ . The green dot in the May subplot of each panel denotes a point  $37^\circ \text{E}$ ,  $3^\circ \text{N}$  which is the model grid point closest to the Turkana area

the larger south-westerly flow (EALLJ; Hart et al. 1978). This splitting is first seen in May, as evident in Fig. 2a–c (May panel in ERA5, MERRA2 and the HadGEM-GC31). The north-easterly stream forms the TJ with a clearer axis from southeast to northwest first seen in April and October in ERA5, MERRA2 and the HadGEM-GC31 model. The BCC-ESM1 model has the TJ merged with the EALLJ, hence the TJ appears to terminate within Turkana region (in

the BCC-ESM1 model). This shortfall appears to be characteristic of most of the models that contribute to the CMIP6 ensemble mean. The spatial structures for other CMIP6 models are shown and discussed in the subsequent subsection of this paper.

The southerly winds carry more moisture into the region during northern summertime compared to other months of the year (Fig. 2). The southerly flow has its sources in the

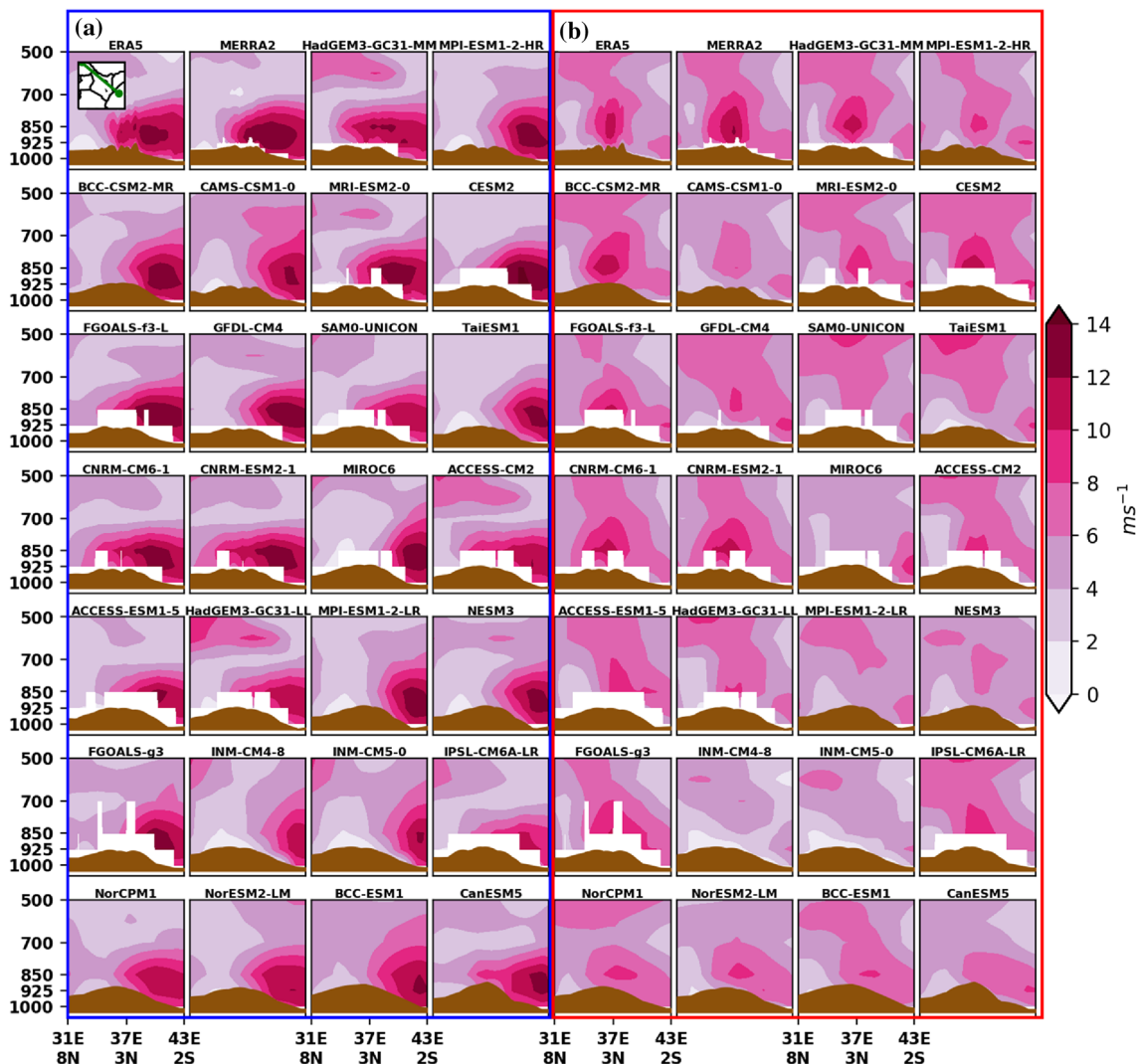


**Fig. 3** Vertical cross-section of climatological mean wind speed (m/s) for June to September (left plot) and October to May (right plot) for the years 1980–2014. Cross-sections are drawn for transect parallel to Turkana channel in Northwest (31° E and 8° N) to Southeast (43° E

and 2° S) direction. The transect is shown insert plot a-ERA5 subplot. Topography is illustrated in the bottom of each subplot in brown. Topography is illustrated in the bottom of each subplot in brown

ocean hence it is laden with more moisture compared to other months when the flow is northerly. The reanalysis and the HadGEM-GC31, having relatively stronger TJ as previously discussed, are indicating higher moisture fluxes during period. In the BCC model, high wind speeds at the entrance, do not extend to mid-Turkana channel as far as HadGEM winds do (Fig. 3). Further analysis (not shown) has also indicated that BCC wind speeds drop off more than HadGEM in climatology and therefore, moisture fluxes in the BCC is lesser in Fig. 2. This period coincides with when the regions bordering the northwest of Kenya receives extended rainfall (Camberlin 2018). Considering the TJ is a major transporting agent for moisture into northwest of East Africa (Vizy and Cook 2019; Munday et al. 2021), simulated impacts of the TJ to rainfall are likely to be different in the reanalysis

and in the CMIP6 models that show a weaker TJ during the season.

### 3.2 Spatial Structure in climatology of the TJ in CMIP6

The mean vertical structure of the lower atmosphere (surface to 500 mb pressure level) winds is analyzed along the Turkana channel in CMIP6 models (Fig. 3). JJAS (Fig. 3a) represents an important study period in which the southerly background flow is split into the TJ and the EALLJ by the underlying Turkana channel, and moisture transport into the northwest of East Africa. The center of intensity appears between 925 and 850 mb pressure levels near the middle of the Turkana channel following acceleration at this point



(Patwardhan and Asnani 1999; Indeje et al. 2001). At the mid-Turkana area, the reanalysis (ERA5 and MERRA2) and the CNRM models exhibit the highest change in wind speeds from maximum (approximately 12 m/s) at 850 mb to point of minimum wind speeds (approximately 7 m/s) before 500 mb level is reached.

Other models with relatively larger changes with height, of more than 5 m/s include HadGEM3-GC31-MM, MRI-ESM2-0, CESM2, FGOALS-f3-L, SAM0-UNICON, ACCESS-CM2, HadGEM3-GC31-LL, IPSL-CM6A-LR and CanESM5. The rest of the models show lower wind shears as mean winds are slower at the mid-Turkana channel. They further show the center of intensity further away from the middle area of the Turkana channel. These models are namely BCC-ESM1, CAMS-CSM1-0, SAM0-UNICON, TaiESM1, MIROC6, NESM3, INM-CM4-8, and INM-CM5-0. In the models, high wind speeds fail to extend up to mid-Turkana Channel, an apparent consequence of the TJ merging with the EALLJ during the JJAS season.

During the October to May months, the EALLJ is absent, the center of intensity in the wind speeds shifts northwards to mid-channel area, it is elevated, and has a vertical elongation up to about 800 mb (Fig. 3b). The vertical extension of the TJ core is accompanied by weaker vertical wind shear. The weakening shear with height appears pronounced in a set of models which exhibited the center of intensity further away from the middle area of the Turkana channel during JJAS season (BCC-ESM1, CAMS-CSM1-0, SAM0-UNICON, TaiESM1, MIROC6, NESM3, INM-CM4-8, and INM-CM5-0). This phenomenon is an indication that while the winds begin to accelerate at mid-Turkana channel, the gain in wind speed is lesser in these models compared to the reanalysis.

The CMIP6 models which have slower winds in the lower-atmosphere, are of relatively lower resolution. Considering that a TJ characterized by high wind speeds that decrease aloft result from acceleration within the Turkana channel, the disparities between the ERA5 and some of the CMIP6 models are likely to result from TJ interaction with topography within the channel.

### 3.3 Mean vertical flow in the Turkana channel

Figure 4 shows the mean omega through the study period, plotted for the northwest to southeast axis parallel to the Turkana channel (for models with the omega data available and the same transect is used as in Fig. 3). Negative (positive) omega values depict ascending (descending) motions. Descending motions dominate the entrance of the Turkana channel during the JJAS season and the mid-channel area during the months of October to May in CMIP6 models. Relating these results with those in Fig. 3 shows that descending motions dominate lower atmospheric

levels where the intensity of the TJ is strong. The ERA5, HadGEM-GC31-LL and the two versions of CNRM model have relatively faster winds at mid-Turkana area during JJAS season following intense TJ core in the season.

Additionally, the influence of the elevated terrain is noticeable. In both the JJAS and October to May seasons, ascending motion emanates between the entrance and the mid-channel area where the floor of Turkana channel begins depicting an elevation, due to frictional interaction of the wind with the sloping floor of the Turkana channel. During JJAS season the TJ core accompanied by subsidence aloft is further to the southeast of the mid-Turkana channel. This allows low-level ascents manifesting at the TJ entrance to incline towards the middle and exit area of the channel with height as generation of the ascents diminish as surface elevation slopes downwards at Turkana channel exit. This further strengthens uplifts at the exit area in the deep troposphere. During October to May months, the TJ core accompanied by subsidence aloft is at the mid-Turkana channel area. Thus, ascents from the TJ entrance area are inhibited from lateral movement towards the mid-Turkana area. At TJ exit, vertical motions are generated by deceleration of winds that leads to build up of pressure at lower atmosphere.

Other than the ERA5 and the two CNRM models, other CMIP6 models show stronger ascending motion, potentially from enhanced blocked lower atmospheric flow at the mid-Turkana channel. The ERA5, HadGEM-GC31 and CNRM models appear to depict unblocked flow through the channel with pockets of near surface descending motion associated with faster wind speeds at the mid-Turkana channel area. During the months of October to May, the mid-channel descents are stronger. This suggests that although strong TJ intensity induces the subsidence in the Turkana channel, the interaction between the TJ and the Turkana channel influences the intensity of the TJ core.

### 3.4 Topography in CMIP6

Figure 5a shows that the Turkana channel is the largest topographic feature below the 850 mb level within the study area bounded by longitudes 33° E and 41° E and latitudes 2° S and 9° N. The floor of the channel at the entrance is roughly at 980 mb in ERA5 and the CMIP6 models. The channel floor rises gently and occupies a varied level of between 945 and 960 mb, matched with high walls at 915 mb in the reanalysis and the models with less than 1° grid step size. In coarser resolution models, the floor of the channel rises to higher level that is fairly similar, approximately at 930 mb. Therefore, the channel appears flattened in them. The CanESM5 and the BCC-ESM1 models have floor of the channel in them, higher above 850 mb.

Figure 5b shows the cross-section of the Turkana channel at each longitude. The channel narrows from about 700

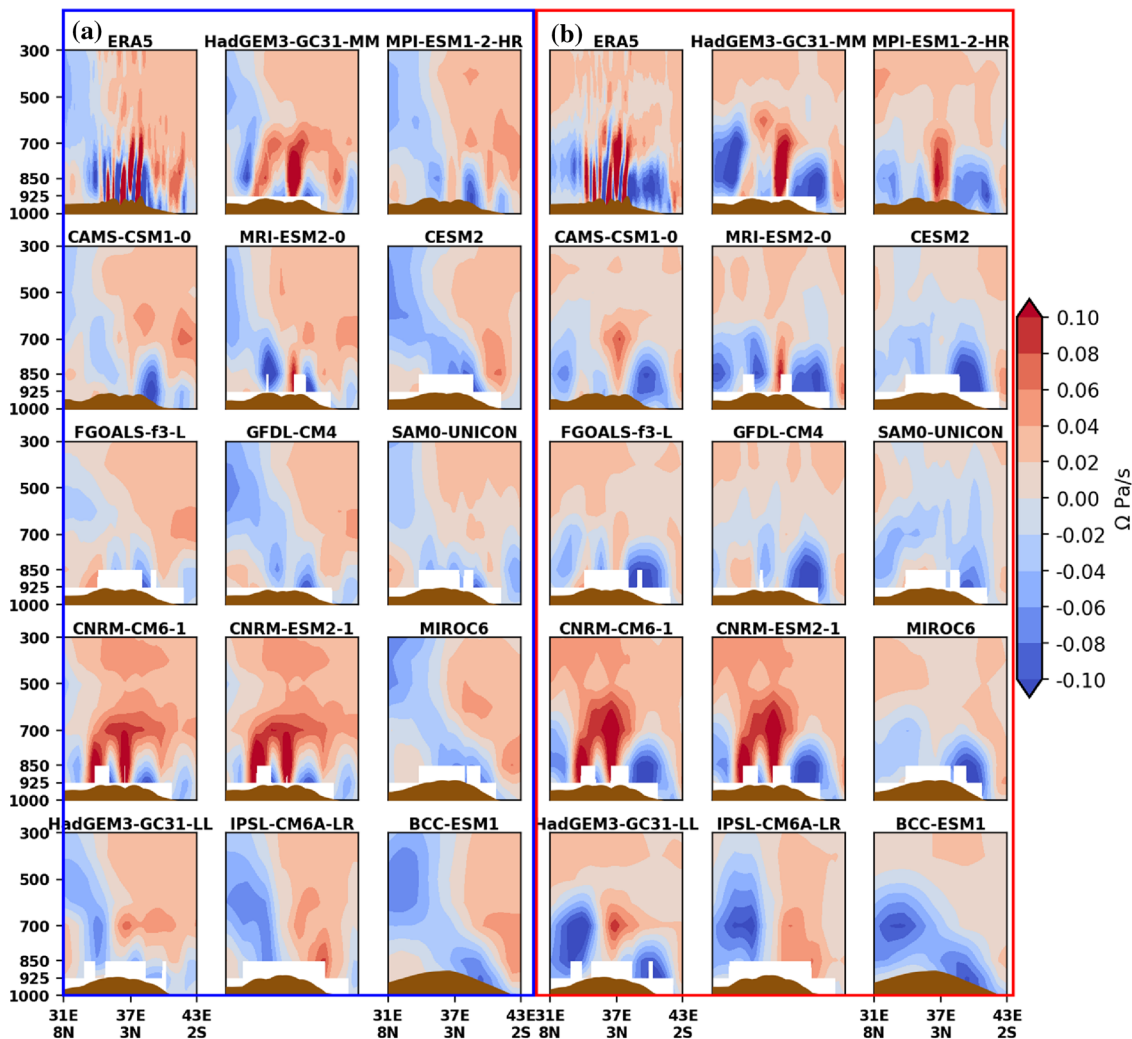


**Fig. 4** Vertical cross-section of climatological mean omega (Pa/s) for June to September (left plot) and October to May (right plot) for the years 1980–2014. Cross-sections are drawn for transect parallel

to Turkana channel in Northwest ( $31^{\circ}$  E and  $8^{\circ}$  N) to Southeast ( $43^{\circ}$  E and  $2^{\circ}$  S) direction, like that used to develop Fig. 3. Topography is illustrated in the bottom of each subplot in brown

square kilometers in the reanalysis (ERA5 and MERRA2) and about 600 square kilometers in CMIP6 models at  $41^{\circ}$  E longitude within  $2^{\circ}$  S and  $9^{\circ}$  N latitudes. The models and the reanalysis attain a restriction at  $37^{\circ}$  E, and the constriction is prominent in the reanalysis plus about half of the models. The INM, NorCPM1 and NorESM2-LM models attain this constriction at  $38^{\circ}$  E. Exiting at the  $37^{\circ}$  E longitude. The channel widens to about 200 square kilometers further to the west of this longitude according to most of the models, other than the CanESM5 and the BCC-ESM1. The 2 models have an apparent exit of the channel at  $35^{\circ}$  E. Through the Turkana channel, the reanalysis and some models (HadGEM-GC31-MM, MPI-ESM1-2-HR, BCC-CSM2, CAMS-CSM1, MRI-ESM2, CESM2) exhibit a wider channel at  $36^{\circ}$  E. The feature becomes prominent when the model

has a higher resolution. As such the ERA5 which has the highest resolution ( $0.25^{\circ}$ ) prominently shows the widening.

While the narrowing of the topography within this area results in the formation of a constriction at the  $37^{\circ}$  E longitude, the consistency in the narrowing (changes between adjacent cross sections) is varied in CMIP6 models compared to the reanalysis. Other than the HadGEM3-GC31-MM and MPI-ESM1-HR models, cross-sectional areas at some adjacent longitudes are maintained or least changed compared to the ERA5. Strikingly, CanESM5 exhibits higher cross-sectional area changes whenever a difference is observed at its relatively coarse spatial grid resolution. The results from ERA5, MERRA2 and the HadGEM3-GC31-MM and MPI-ESM1-HR which are two high-resolution CMIP6 models show that reducing the grid-step size increases topographic details being resolved and forms a

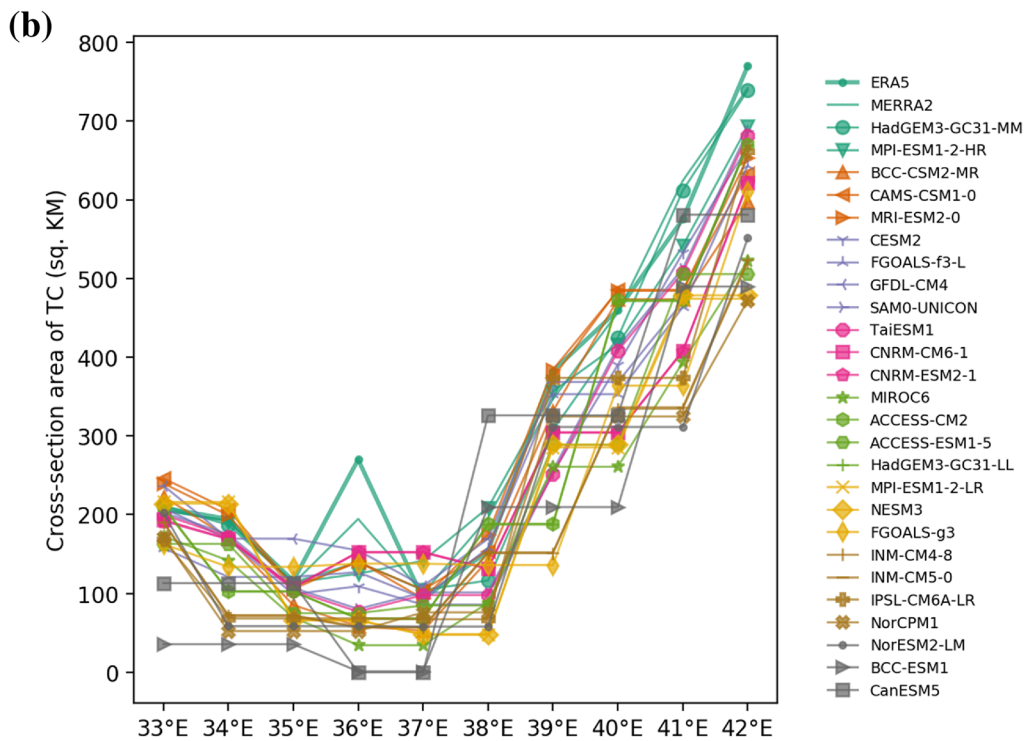
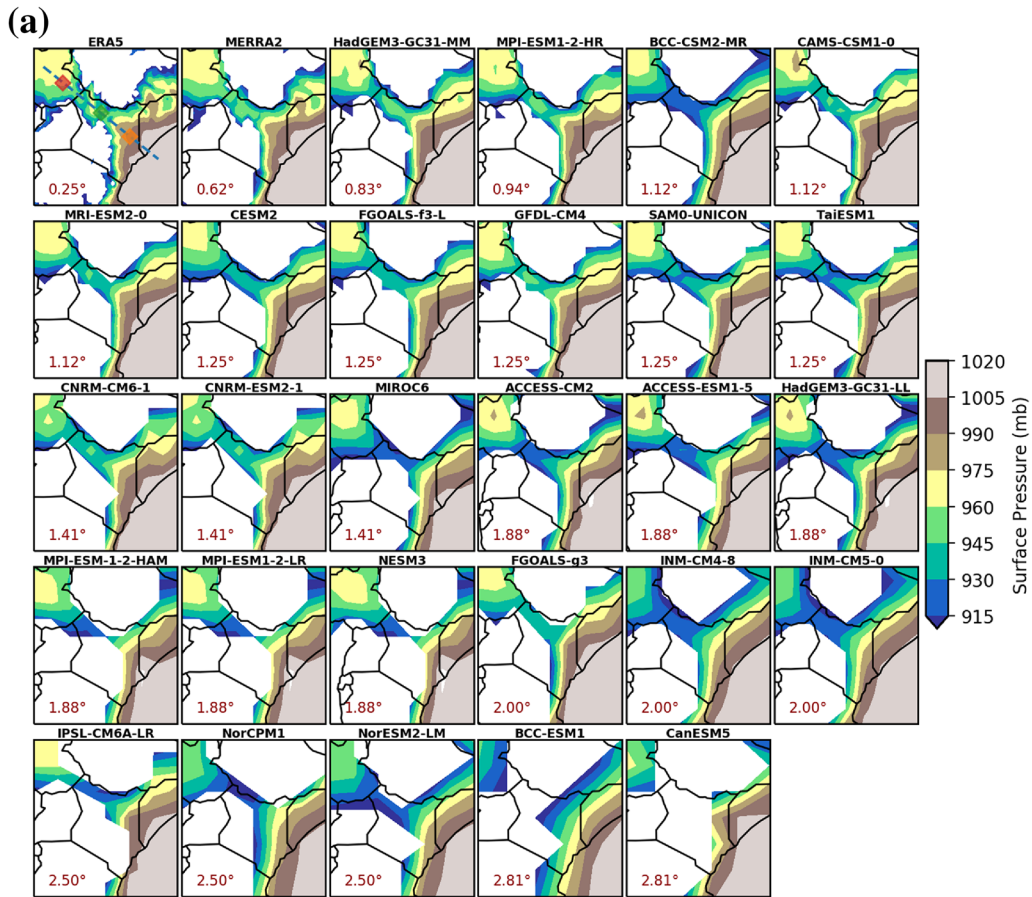


**Fig. 5** **a** Surface elevation in ERA5, MERRA2 and the CMIP6 models over the Turkana channel area, with elevation above 850 mb level masked out. The in-plot texts indicate the model longitudinal grid step size. The blue dotted line in the ERA5 panel show a transect parallel to the Turkana Channel in Southeast (entrance; orange) to Northwest (exit; red) direction through a point at center of the channel (green; 37° E and 3° N). The area bordering Tanzania, Kenya and Somalia on their eastmost boundary, is below sea-level (1000 mb) while white patches show elevation above 850 mb level. **b** Estimated cross sectional area of Turkana Channel (in square kilometers) at each longitude between latitudes 2° S and 9° N. The quantity is abbreviated as TC

narrowing Turkana channel. The narrowing phenomenon has been used to explain existence of a faster TJ in MERRA2 as it has a consistently narrowing channel (Vizy and Cook 2019). The next step of this analysis explores how these finer details of the topography relates with the representation of the TJ.

The difference between the cross-sectional area of the channel at the entrance and exit of the jet is computed. Figure 6 shows the narrowing index for CMIP6 models as well as the horizontal resolution (longitudinal grid step size) of the model. Since the cross-sectional area entrance of the channel (42°E) in the ERA5 and all the CMIP6 models is about 800 square kilometers and reduces to about an eighth of this at the mid-channel, models with zero changes between adjacent longitudes have higher gradient whenever shape changes. Thus, a low index (Fig. 6, y-axis), which is characteristic of low-resolution models with higher grid step sizes, characterizes steep change in terrain followed by blocks of wall between the adjacent longitudes with constant cross-section area between them.

The ERA5 has the highest narrowing index for the Turkana channel. It is followed by CMIP6 models of less than 1.5° resolution in which the index is either maintained or weakens in models with higher grid-step sizes. At greater than 1.5° resolution, the CMIP6 models scattered values for the index and show inconsistency in how the narrowing of the channel is lost with increasing coarseness in the topography. The CanESM5 model is an outlier, returning a high value of the quantity due to high rates of change associated with very large grid-step sizes and a smaller number of points in the channel (Fig. 5b). Therefore, linking this result with those from Fig. 3 indicates that CMIP6 models with resolution greater than 1.5° have steep walls along the floor and height of the channel. This is a likely source of the impediment on the smooth flow near the surface along the Turkana channel.

### 3.5 Topographic influence on the TJ in CMIP6

The association between the strength of the TJ and the shape of the Turkana channel represented by the narrowing index, is explored in this section by adjusting the thresholds

for JJAS season maximum wind speed and vertical shear (between the point of maximum and minimum wind speed before reaching 500 mb). Figure 7 shows TJ counts for wind speeds at 850 mb in range 6–10 m/s and wind shear above the TJ core in range 2–6 m/s, for each model and its narrowing index.

Most models return a TJ with maximum wind speeds exceeding 6 m/s and vertical wind shear above the TJ core exceeding 2 m/s. Only INM and ACCESS-ESM models have the TJ structure weaker than this category within the 35-year study period. Higher thresholds of 9 m/s at 850 mb and vertical wind shear of 5 m/s TJs are most common in the majority (17) of the 26 CMIP6 models. At a level higher (9 m/s maximum wind speeds and greater than 6 m/s vertical shears above the TJ core), a robust positive correlation exists between the TJ counts and the narrowing index. At this point, the criteria are stricter and nearly half of the CMIP6 models return zero TJ counts. Therefore, we consider those thresholds as optimal.

The optimum thresholds are surpassed in CMIP6 models having a high narrowing index such as HadGEM3-GC31-MM, CNRM and MRI. This is similar to the ERA5 which has the highest index (Fig. 6) considering TJs whose core is characterized by at least 9 m/s maximum wind speeds which decrease by at least 5 m/s above. Referring to Fig. 3, the mean TJ in ERA5 reaches higher values for maximum wind speeds at 12 m/s, decreasing by 7 m/s above the core. CMIP6 models with lower narrowing index exhibit mixed TJ characteristics. For instance, the CNRM and FGOALS-f3-L models exhibit TJs when NorESM2-LM and INM models of comparable index, return zero TJ count considering the optimum thresholds for the TJ in CMIP6 models. There were 9 CMIP6 models with zero TJs and 4 models with 35 TJs reaching the optimum threshold in 35 JJAS seasons. The remaining 13 CMIP6 models occasionally exhibited TJs reaching the optimum threshold for a strong jet (maximum wind speeds of 9 m/s and decreasing aloft the core by at least 5 m/s).

The different CMIP6 models (coarser than 1.5° longitudinal resolution) with low narrowing index show a lower consistency in narrowing cross sectional area. Considering that the narrowing supports channeling of the winds and acceleration of the winds (Indeje et al. 2001), models with coarser than 1.5° longitudinal grid step size which occasionally exhibit weak TJ structure, are here found to be related to poor resolution of the Turkana channel. These irregularities in the TJ strength could also influence rainfall at TJ exit, as the TJ is considered a moisture transport mechanism (Munday et al. 2021).

**Fig. 6** Mean zonal change in cross-sectional area of Turkana channel estimated between longitudes 33° E and 42° E, each longitude spanning between latitudes 2° S and 9° N; referred to as the narrowing index in this paper. The quantity is computed for different models on their native grid whose longitude grid spacing are shown in the x-axis. The Pearson product moment correlation coefficient ( $\rho$ ) between the narrowing index and the horizontal grid resolution shows significant correlation at the 95% confidence level ( $p$ -value < 0.05)

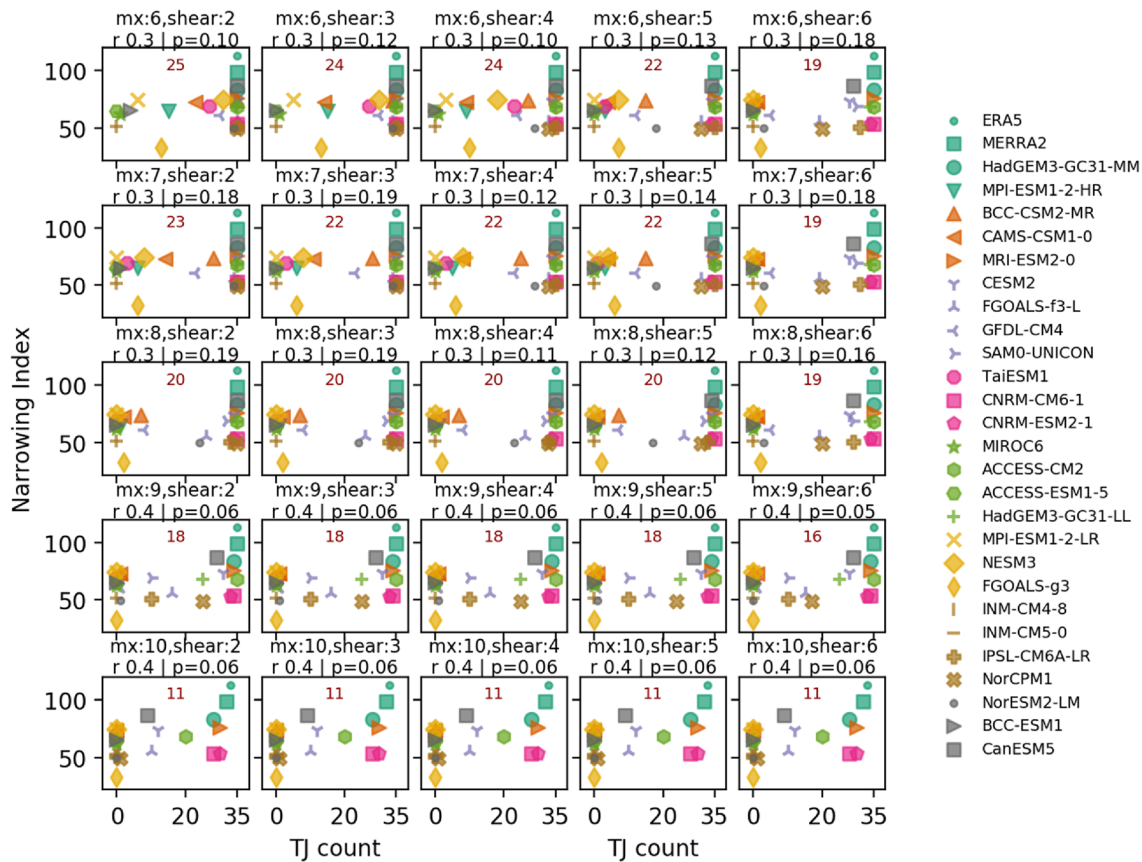
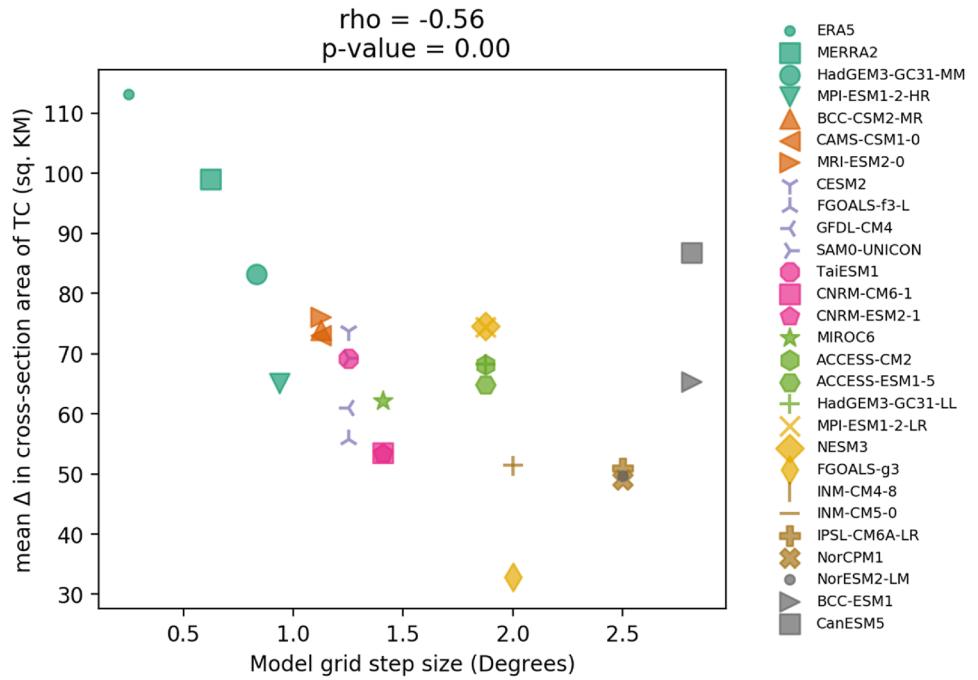


**Fig. 7** Dependence of the TJ occurrence on the narrowing index. Counts are made for the TJ of maximum wind speeds and highest decrease between 850mb and point of minimum below 500 mb, shown in the title of each subplot. Also shown in text are spearman's

rank correlation and p-value between TJ counts and narrowing index. The number of models returning more than zero (0) TJ count is shown in inner text

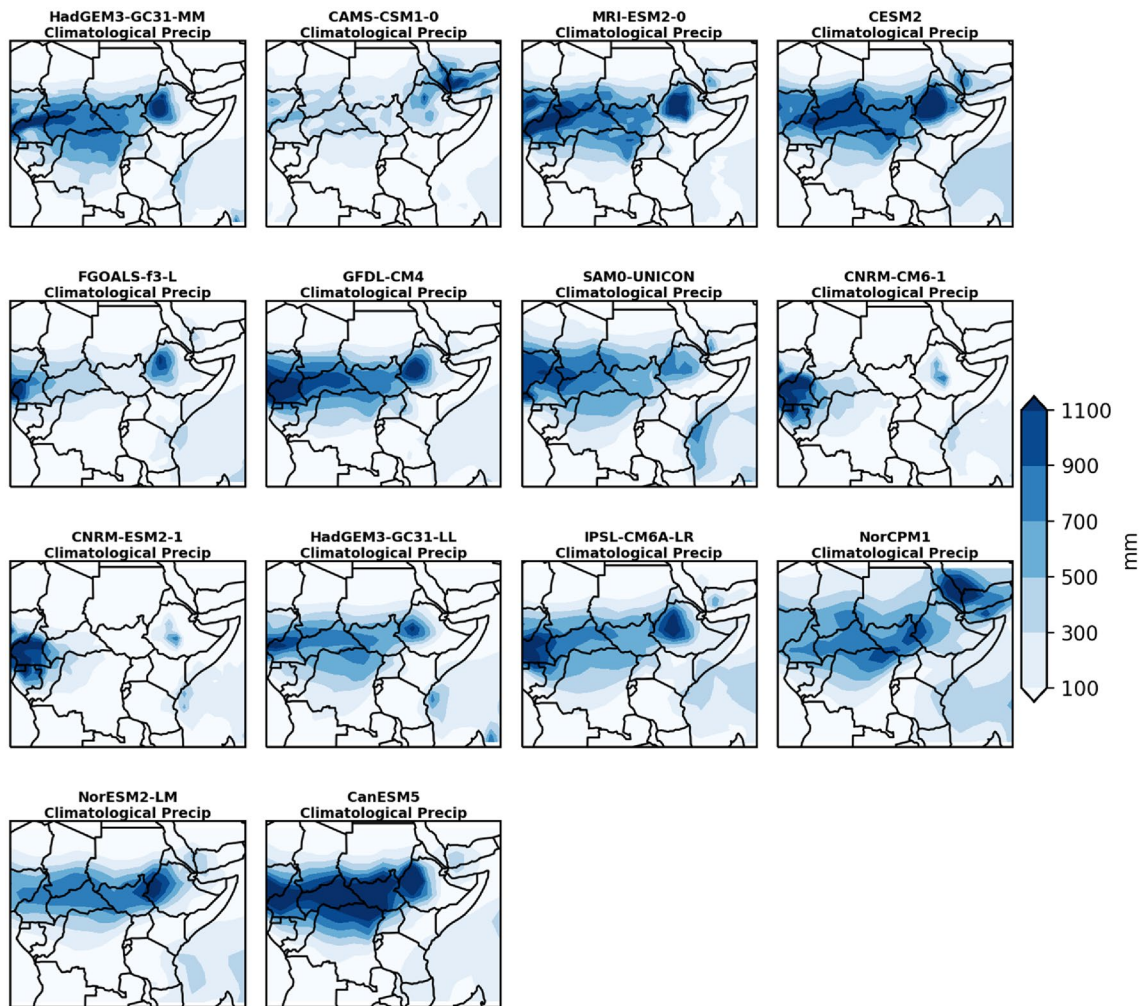


Fig. 8 Mean climatological precipitation (mm) during the June to September season for the years 1980–2014

### 3.6 Relationship between TJ and East African Precipitation in CMIP6

The influence of the TJ on the climate of East Africa precipitation is investigated in the JJAS season for CMIP6 models having an irregular TJ (Fig. 8). In the models, JJAS is a major season with rainfall accumulation of up to 1100 mm over the northwest regions of East Africa, particularly over western of Ethiopian highlands. Other areas with similar precipitation amounts include Northern Congo, most of Central African Republic and the west of South Sudan in CanESM1 and lesser magnitude (900 mm) over these areas in GFDL, CESM2, HadGEM (both) MRI, NorESM1, NorCPM1, IPSL and SAM. In those models, areas that border exit of the TJ (northern Kenya boarder with South Sudan) have about 500 mm rainfall within this season, an area which has observed climatological annual rainfall of 700 mm, mainly received in JJAS (Camberlin 2018). In the CAMS, FGOALS, and both versions of CNRM, the areas

at immediate exit of the TJ and most of South Sudan, are drier with less than 300 mm precipitation during this season.

The influence of the TJ on the model climate of East Africa in JJAS, is shown using the composite anomalies of precipitation associated with the TJ (Fig. 9). Mean precipitation anomalies are shown for strong TJs in the CMIP6 models that best match TJ strength in the ERA5 (at least 9 m/s at the 850 mb and vertical wind shear of at least 5 m/s above TJ core) in the “jet” panel and also when the strength was weaker “no jet cases” panel. The climatological conditions of northwestern of East Africa, are also mirrored when the TJ strength is regularly either strong or wet. Fluctuations in the TJ strength which is common in nearly half of the CMIP6 models used, induce spatial distribution of dry and wet anomalies.

In Fig. 9 both versions of CNRM have a regularly strong TJ. In them, high speed winds extend furthest into the channel (Fig. 3) so although it is a high jet count model, it is wetter further west to other models (in Fig. 8). The CanESM

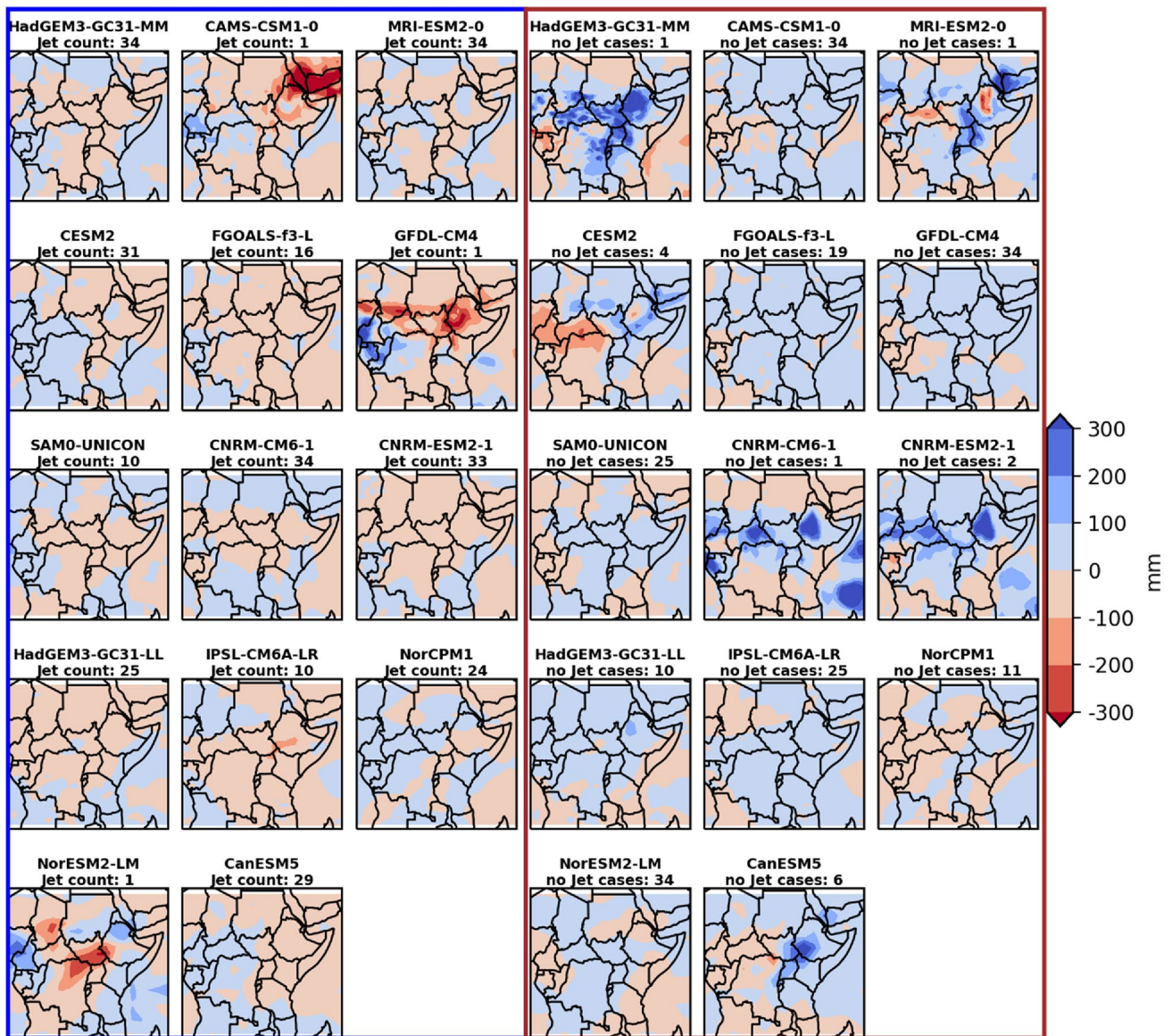


**Fig. 9** Composite anomalies for precipitation during the June to September season for the years 1980–2014. Left panel shows the composite anomalies for jet occurrence (TJ core speeds at least 9 m/s and decreases above the core by at least 5 m/s; JJAS seasons in which

thresholds were met). Right panel shows the composite anomalies for no jet occurrence (TJ core speeds at least 9 m/s and decreases above the core by at least 5 m/s; JJAS seasons in which thresholds were not met)

model equally a regularly strong TJ albeit the high-speed winds do not extend as much compared with CNRM into the channel (Fig. 3) so it is wetter from the immediate exit of the TJ compared to other models (in Fig. 8). Left panel of Fig. 9 shows anomalies associated with the TJ. When a perennially weak TJ strengthens in model climatology, dry anomalies at the border region of the exit the Turkana channel are exhibited. Specifically, rainfall is suppressed by up to 200 mm below the climatological mean, exhibited in CAMS, BCC, GFDL and FGOALS. The dryness extends up to the west of South Sudan, east of Central African Republic,

northern Congo and to the west of Ethiopian Highlands. The increasing dry anomalies at the TJ exit area is associated with stronger inflow of air with low moisture content during this season through lower atmosphere. Furthermore, during a strong TJ, easterly flow is so strong that it inhibits southwesterly advection of moist air from equatorial Congo.

Conversely, wet anomalies characterize the immediate exit of Turkana channel and Ethiopian highlands in the CMIP6 models when perennially strong TJ weakens below the thresholds (Fig. 9; right panel). Precipitation is enhanced by up to 200 mm more than the climatological mean in the models. Further to the west of South Sudan,

in the Central African Republic and northern Congo, dry anomalies below the climatological mean are exhibited. This is likely associated with enhanced uplift of moist air that is transported from the Indian Ocean through the Turkana channel at TJ exit. In this case, pressure piles up at the immediate exit due to deceleration of winds and promotes zonal advection of moisture-laden air to the western regions of South Sudan (Vizy and Cook 2019). Furthermore, during a weak TJ, southwesterly advection of moist air from equatorial Congo is likely being promoted.

#### 4 Summary and conclusions

The TJ is a persistent jet stream that is observed throughout the year in the ERA5 data with seasonal mean wind speeds ranging between 11 and 13 m/s at approximately 850 mb level. However, it varies appreciably in CMIP6 models with typical core speeds ranging between 5 and 9 m/s. The maximum wind speed at the core of the TJ in the ERA5 is highest during May to October months when the background flow is southeasterly, while the majority of the CMIP6 models with coarse resolution show their minimum wind speeds during this period.

The period from June to September is characterized by strong vertical shear above the TJ core at the mid-Turkana channel and the presence of the EALLJ in both the ERA5 and CMIP6 models. In some models the EALLJ dominates, and there are high wind speeds (up to 9 m/s) closer to the entrance of the Turkana channel while the winds at the mid-channel area are too weak by up to 5 m/s. This is an indication that the TJ is merged with the EALLJ, which inhibits the strong winds from reaching mid-Turkana channel. In other months of the year, the EALLJ is inactive and the high wind speeds (up to 9 m/s) are located at mid-Turkana channel signifying the TJ core in CMIP6 models as is in ERA5. Furthermore, the core of the TJ appears vertically extended up to 700 mb in the models and reduces the magnitude of change between maximum wind speed at TJ core and minimum wind speeds found aloft at the mid-channel. The vertical wind profiles are therefore mixed in most CMIP6 models.

Analysis of vertical winds indicate that the mixed profiles of wind speed in the CMIP6 models is potentially related to ascending motion from the mid-Turkana channel that leads to the upward spread of relatively high wind speeds. The upward flow from the mid-channel could be enhanced by frictional interaction with the floor and wall of the Turkana channel and is pronounced in CMIP6 models with horizontal resolution of coarser than  $1.5^\circ$ . The frictional encounter of the wind flow with the floor of the Turkana channel appears as enhanced ascending motion

from blocked flow at mid-Turkana channel. The enhanced ascent due to blocked motion is likely to result in heightening of precipitation. The present analysis depicts that precipitation could be enhanced up to 200 mm in the season at exit of the TJ by the ascents in CMIP6 models with longitudinal grid step size higher than  $1.5^\circ$ .

This study provides insights on the representation of features of the TJ in the available CMIP6 models and reanalysis datasets (ERA5 and MERRA2). The results also reaffirm the importance of the TJ to the climate of East Africa by transporting moisture during the northern summer, an aspect also presented in other studies including Indeje et al. (2001), Nicholson (2016), Vizy and Cook (2019) and King et al. (2021). Additionally, we find that higher resolution CMIP6 models have a better Turkana channel characterized by consistent narrowing along the channel (through the narrowing index) which allows for smooth flow and acceleration of winds at mid-Turkana channel area. The study has demonstrated that for coarse model resolution with a low of at least  $1.5^\circ$ , the narrowing index is low and produces a TJ with high variability in its strength, location of core and vertical structure. The variation in strength, location and structure of the TJ translates to biases in the CMIP6 model rainfall climatology over Eastern Africa, leading to emergence of dry (wet) anomalies over the northwestern region of East Africa when the TJ is strong (weak). The enhancement of wet anomalies is up to 400 mm above the observed climatology at the immediate exit of the TJ when the jet stream is weaker. The area of influence of the TJ borders the drier Sudan to the north, whose annual precipitation, mainly from the JJAS season is lower than 400 mm. Therefore, the TJ is likely to be critical to the climate regime in the relatively wetter areas of northwestern of East Africa, as well as the drier climate of the surrounding.

These findings demonstrate the importance of realistically representing the topography details over the Turkana channel based on an analysis using model data. This highlights the need for field studies to determine a realistic baseline for comparison of the observed climatology of the TJ and the relationship between the TJ and rainfall. While an understanding of the TJ features can be drawn from some low-resolution RA and models (e.g., Nicholson 2016; King et al. 2021), most of them have high variability in seasonal cycle in strength of the TJ in models, which is not being exhibited in the closest to observations dataset. This implies that model information could mislead if used for planning using the wind data. There is still need to postprocess wind and rainfall data from the models over the northern Kenya area especially Turkana channel to remove biases as the TJ provides potential for wind energy, which the government can invest in to supplement energy of sources. There is also the need for increased resolution to realistically represent the



TJ. The narrowing index provides a quantitative way to track improvement of high-resolution modelling to the narrowing shape of the Turkana channel, much needed to realistically represent the structure, position, strength of TJ and influence on rainfall in atmospheric models. The next steps for this work are to apply our findings to models with resolution hierarchy in controlled experiments and further explore the factors responsible for the inter-annual variability of the perennially weak TJ in the CMIP6 models.

**Acknowledgements** This work is part of outputs from the LaunchPAD (Priority on African Diagnostics) project, funded by the Foreign, Commonwealth and Development Office (FCDO) to create a Climate Model Evaluation Hub for Africa. The analysis in this work was done via JASMIN data cluster with datasets. We acknowledge the ECMWF for providing the ERA5 datasets, and the World Climate Research Programme Working Group on Coupled Modeling, for providing CMIP6 datasets to support this research.

**Funding** The research was supported by the Foreign, Commonwealth and Development Office (FCDO).

**Data availability statement** The ERA5 dataset analyzed in this work are available through, <https://cds.climate.copernicus.eu/cdsapp#!/home> and CMIP6 data through the Centre for Environmental Data Analysis (CEDA), available here <https://catalogue.ceda.ac.uk/uuid/b96ce180077f4810abc4eef0e48901d9>.

## Declarations

**Conflict of interest** The authors have not disclosed any competing interests.

**Open Access** This article is licensed under a Creative Commons Attribution 4.0 International License, which permits use, sharing, adaptation, distribution and reproduction in any medium or format, as long as you give appropriate credit to the original author(s) and the source, provide a link to the Creative Commons licence, and indicate if changes were made. The images or other third party material in this article are included in the article's Creative Commons licence, unless indicated otherwise in a credit line to the material. If material is not included in the article's Creative Commons licence and your intended use is not permitted by statutory regulation or exceeds the permitted use, you will need to obtain permission directly from the copyright holder. To view a copy of this licence, visit <http://creativecommons.org/licenses/by/4.0/>.

## References

- Acosta RP, Huber M (2017) The neglected Indo-Gangetic Plains low-level jet and its importance for moisture transport and precipitation during the peak summer monsoon. *Geophys Res Lett* 44(16):8601–8610. <https://doi.org/10.1002/2017gl074440>
- Ba MB, Nicholson SE (1998) Analysis of convective activity and its relationship to the rainfall over the Rift Valley lakes of East Africa during 1983–1990 using the METEOSAT infrared channel. *J Clim Appl Meteorol* 10:1250–1264
- Cam Eyring V, Bony S, Meehl GA, Senior CA, Stevens B, Stouffer RJ, Taylor KE (2016) Overview of the Coupled Model Inter-comparison Project Phase 6 (CMIP6) experimental design and organization. *Geosci Model Dev* 9:1937–1958. <https://doi.org/10.5194/gmd-9-1937-2016>
- Camberlin P (2018) Climate of Eastern Africa. In: Oxford research encyclopedia of climate science. Oxford University Press, Oxford
- Hart JE, Rao GV, Van De Boogaard H, Young JA, Findlater J (1978) Aerial observations of the East African low-level jet stream. *Mon Weather Rev* 106(12):1714–1724
- Hartman AT (2018) An analysis of the effects of temperatures and circulations on the strength of the low-level jet in the Turkana Channel in East Africa. *Theor Appl Climatol* 132:1003–1017. <https://doi.org/10.1007/s00704-017-2121-x>
- Hersbach H, Bell B, Berrisford P, Hirahara S, Horányi A, Muñoz-Sabater J, Nicolas J, Peubey C, Radu R, Schepers D, Simmons A, Soci C, Abdalla S, Abellan X, Balsamo G, Bechtold P, Biavati G, Bidlot J, Bonavita M, De Chiara G, Dahlgren P, Dee D, Diamantakis M, Dragani R, Flemming J, Forbes R, Fuentes M, Geer A, Haimberger L, Healy S, Hogan RJ, Hólm E, Janisková M, Keeley S, Laloyaux P, Lopez P, Lupu C, Radnoti G, de Rosnay P, Rozum I, Vamborg F, Villaume S, Thépaut JN (2020) The ERA5 global reanalysis. *Q J R Meteorol Soc*. <https://doi.org/10.1002/qj.3803>
- Indeje M, Semazzi FHM, Xie L, Ogallo LJ (2001) Mechanistic model simulations of the East African climate using NCAR regional climate model: influence of large-scale orography on the Turkana low-level jet. *J Clim* 14:2710–2724
- James R, Washington R, Abiodun B, Kay G, Mutemi J, Pokam W, Hart N, Artan G, Senior C (2017) Evaluating climate models with an African lens. *Bull Am Meteorol Soc* 1:1. <https://doi.org/10.1175/BAMS-D-16-0090.1>
- Kilavi M, MacLeod D, Ambani M, Robbins J, Dankers R, Graham R, Todd M (2018) Extreme rainfall and flooding over Central Kenya including Nairobi City during the Long-Rains season 2018: causes, predictability, and potential for early warning and actions. *Atmosphere* 9(12):472. <https://doi.org/10.3390/atmos9120472>
- King JA, Washington R, Engelstaedter S (2020) Representation of the Indian Ocean Walker circulation in climate models and links to Kenyan rainfall. *Int J Climatol*. <https://doi.org/10.1002/joc.6714>
- King JA, Engelstaedter S, Washington R, Munday C (2021) Variability of the Turkana low-level jet in reanalysis and models: Implications for rainfall. *J Geophys Res Atmos* 126:e2020JD034154. <https://doi.org/10.1029/2020JD034154>
- Kinuthia JH (1992) Horizontal and vertical structure of the Lake Turkana Jet. *J Appl Meteorol* 31:1248–1274
- Kinuthia JH, Asnani GC (1982) A newly found jet in North Kenya (Turkana Channel). *Mon Weather Rev* 10:1722–1728
- McGregor S, Timmermann A, Stuecker MF, England MH, Merrifield M, Jin F-F, Chikamoto Y (2014) Recent Walker circulation strengthening and Pacific cooling amplified by Atlantic warming. *Nat Clim Chang* 4:888–892. <https://doi.org/10.1038/nclimate2330>
- Munday C, Washington R, Hart N (2021) African low-level jets and their importance for water vapor transport and rainfall. *Geophys Res Lett* 48:e2020GL090999. <https://doi.org/10.1029/2020GL090999>
- Nicholson SE (1996) A review of climate dynamics and climate variability in eastern Africa. In: Johnson TC, Odada EO (eds) *The limnology, climatology and paleoclimatology of the East African Lakes*. Gordon and Breach, Toronto, pp 25–56
- Nicholson SE (2014) The predictability of rainfall over the Greater Horn of Africa. Part I. Prediction of seasonal rainfall. *J Hydrometeorol* 33:1011–1027. <https://doi.org/10.1175/JHM-D112913-062.1>
- Nicholson SE (2016) The Turkana low-level jet: mean climatology and association with regional aridity. *Int J Climatol* 36:2598–2614. <https://doi.org/10.1002/joc.4515>

- Njenga M, Leeuw J, O'Neill M, Ebanyat P, Kinyanjui M, Kimeu P, Adirizak H, Sijmons K, Vrieling A, Malesu M, Oduor A, Dobie P (2014) The need for resilience in the drylands of Eastern Africa. In: Leeuw J, Njenga M, Wagner B, Iiyama M (eds) *Treesilience: an assessment of the resilience provided by trees in the drylands of Eastern Africa*. World Agroforestry Centre Nairobi, Nairobi. <https://doi.org/10.13140/2.1.4118.5927>
- Oliveira MI, Nascimento EL, Kannenberg C (2018) A New Look at the Identification of Low-Level Jets in South America. *Mon Weather Rev* 146(7):2315–2334
- Patwardhan SK, Asnani GC (1999) Meso-scale distribution of summer monsoon rainfall near the western Ghats (India). *Int J Climatol* 20:575–581
- Philip S, Kew SF, van Oldenborgh GJ, Otto F, O'Keefe S, Hausteine K, King A, Zegeye A, Eshetu Z, Hailemariam K, Singh R, Jjemba E, Funk C, Cullen H (2018) Attribution analysis of the Ethiopian drought of 2015. *J Clim* 31(6):2465–2486. <https://doi.org/10.1175/JCLI-D-17-0274.1>
- Preethi B, Sabin TP, Adedoyin JA, Ashok K (2015) Impacts of the ENSO-Modoki and other tropical Indo-Pacific climate drivers on African rainfall. *Sci Rep*. <https://doi.org/10.1038/srep16653>
- Slingo J, Spencer H, Hoskins B, Berrisford P, Black E (2005) The meteorology of the Western Indian Ocean, and the influence of the East African Highlands. *Philos Trans R Soc Lond A Math Phys Eng Sci* 363(1826):25–42
- Sun LQ, Semazzi FHM, Giorgi F, Ogallo L (1999) Application of the NCAR regional climate model to eastern Africa—1. Simulation of the short rains of 1988. *J Geophys Res Atmos* 104:6529–6548
- Taylor KE, Stouffer RJ, Meehl GA (2012) An overview of CMIP6 and the experimental design. *B Am Meteorol Soc* 93:485–498. <https://doi.org/10.1175/BAMS-D-11-00094.1>
- Trewartha GT (1981) *The Earth's problem climates*. University of Wisconsin Press, Madison, p 340
- Uhe P, Philip S, Kew S, Shah K, Kimutai J, Mwangi E, Jjemba E (2018) Attributing drivers of the 2016 Kenyan drought. *Int J Climatol* 38:554–568
- Vizy EK, Cook KH (2019) Observed relationship between the Turkana low-level jet and boreal summer convection. *Clim Dyn* 53:4037–4058. <https://doi.org/10.1007/s00382-019-04769-2>
- Yang W, Seager R, Cane MA, Lyon B (2015) The rainfall annual cycle bias over East Africa in CMIP5 coupled climate models. *J Clim* 28(24):9789–9802. <https://doi.org/10.1175/jcli-d-15-0323.1>

**Publisher's Note** Springer Nature remains neutral with regard to jurisdictional claims in published maps and institutional affiliations.